Revision_1

Minerals in cement chemistry: a single-crystal neutron diffraction study of ettringite, $Ca_6Al_2(SO_4)_3(OH)_{12}\cdot 27H_2O$

G. Diego Gatta[1,2], Ulf Hålenius [3], Ferdinando Bosi[4],

Laura Cañadillas-Delgado[5,6], Maria Teresa Fernandez-Diaz[5]

[1] Dipartimento di Scienze della Terra, Università degli Studi di Milano, Via Botticelli 23, I-20133 Milano, Italy

[2] CNR-Istituto di Cristallografia, Via Amendola 22/O, I-70126 Bari, Italy

[3,4]Department of Geosciences Swedish Museum of Natural History, P.O. Box 50 007, SE-104 05 Stockholm, Sweden

[4]Department of Earth Sciences, Sapienza University di Rome, Piazzale A. Moro 5, I-00185, Roma, Italy

[5]Institut Laue-Langevin, 71 Avenue des Martyrs, F-38000 Grenoble, France

[6]Centro Universitario de la Defensa de Zaragoza, ctra Huesca s/n, 50090 Zaragoza, Spain

Corresponding author: diego.gatta@unimi.it

Abstract

Ettringite, ideally $Ca_6Al_2(SO_4)_3(OH)_{12}\cdot 26H_2O$, is recognized as a secondary-alteration mineral and as an important crystalline constituent of the Portland cements, playing different roles at different time scales. It contains more than 40 wt% of H_2O. The crystal structure and crystal chemistry of ettringite were investigated by electron microprobe analysis in wavelength-dispersive mode, infrared spectroscopy and single-crystal neutron diffraction at 20 K. The anisotropic neutron structure refinement allowed the location of (22+2) independent H sites, the description of their anisotropic vibrational regime and the complex H-bonding schemes. Analysis of the difference-Fourier maps of the nuclear density showed a disordered distribution of the inter-column ("free") H_2O molecules of the ettringite structure, modelled (in the structure refinement) with two independent and mutually exclusive configurations. As the disorder is still preserved down to 20 K, we are inclined to consider that as a "static disorder". The structure of ettringite is largely held together by hydrogen bonding: the building units [*i.e.*, SO_4 tetrahedra, $Al(OH)_6$ octahedra and $Ca(OH)_4(H_2O)_4$ polyhedra] are interconnected

through extensive network of hydrogen bonds. The ettringite of this study has an almost ideal composition, with 27 H_2O molecules per formula unit and (Mn+Fe+Si+Ti+Na+Ba) < 0.04 atoms per formula unit. The effect of the low-temperature stability of ettringite and thaumasite on the pronounced "Sulphate Attack" of Portland cements, observed in cold regions, is discussed.

Key-words: ettringite, Portland cements, crystal chemistry, single-crystal neutron diffraction, infrared spectroscopy, hydrogen bonding.

Introduction

Ettringite, with ideal chemical formula reported in the literature $Ca_6Al_2(SO_4)_3(OH)_{12}\cdot 26H_2O$ [$a \sim 11.2$ Å, $c \sim 21.3$ Å, space group $P31c$ or $P6_3/mcm$, $Z = 2$], occurs in metamorphosed limestone (near igneous contacts or in xenoliths) or as a low-temperature secondary-alteration phase (*e.g.*, weathering crusts on larnite rocks), usually associated with portlandite, afwillite, hydrocalumite afwillite, hydrocalumite, mayenite, and gypsum. It is expected to form a solid solution with thaumasite, $Ca_3Si(OH)_6(CO_3)(SO_4)\cdot 12H_2O$ (Moore and Taylor 1970; Barnett et al. 2000).

More than in Nature, an ettringite-like phase is an important crystalline constituent of the Portland cements, and it plays different roles at different time scales. In early hydration stages, the crystallization of ettringite governs the set rate of the calcium aluminate phase ("C3A", $Ca_3Al_2O_6$), which is highly reactive (Taylor 1997; Renaudin et al. 2007). In aged cements, delayed formation of ettringite and thaumasite can promote destructive processes, especially in cement products in which limestone is used as a filling material (Hartshorn et al. 1999) and a diffusion of sulphate-rich fluids occurs (*e.g.*, by contact with sulphate-rich soils or groundwater) (Crammond 1985). The

main cement hydration products, *i.e.*, calcium silicate or aluminate hydrates (the so-called C-S-H and C-A-H) and calcium hydroxide (portlandite $Ca(OH)_2$), are decomposed as a result of both sulphate attack and carbonation: as C-S-H and C-A-H provide most of the binding strength, the formation of ettringite and thaumasite leads to weakening and disintegration of the cement matrix. This phenomenon is more pronounced in cement structures below ground (*e.g.*, Hartshorn et al. 1999; Bensted 1999; Hobbs and Taylor 2000; Santhanam et al. 2001; Zhang et al. 2009; Gatta et al. 2012). The effect of carbonate ions on delayed ettringite formation was recently reported by Asamoto et al. (2017).

The crystalline structure of ettringite has been previously investigated by several authors by single-crystal or powder X-ray diffraction (*e.g.*, Moore and Taylor 1968, 1970; Goetz-Neunhoeffer and Neubauer 2006) and by neutron powder diffraction (Hartman and Berliner 2006). Its crystal structure is significantly complex (Fig. 1): it consists of $[Ca_3[Al(OH)_6]\cdot 12H_2O]$-columns, parallel to [001], and connected by sulphate groups *via* hydrogen bonds with H_2O molecules. In each column, $Al(OH)_6$-octahedra alternate with triplets of calcium polyhedra with coordination number CN = 8, *i.e.*, coordinated by 4 (OH)-groups and 4 H_2O molecules disposed around the 3-fold axis. Disordered distribution affecting the inter-column H_2O molecules was reported and even the disordered distribution of the building groups would lead to a different symmetry of the structure (Moore and Taylor 1970). The structure of a synthetic ettringite-type compound, $Ca_6[Al(OD)_6]_2(SO_4)_3\cdot 25.5D_2O$, was re-investigated by Hartman and Berliner (2006) by neutron powder diffraction. The authors were able to locate the proton sites with a structure model in the space group *P*31*c*. However, all the sites were modelled isotropically, with unusually different displacement factors for

atoms of the same ionic groups, and some of the refined site occupancy factors showing partial occupancies.

The aforementioned studies, along with those conducted on the thermal and compressional behaviour of ettringite (*e.g.*, Skoblinskaya and Krasilnikov 1975; Skoblinskaya et al. 1975; Zhou and Glasser 2001; Deb et al. 2003; Hartman et al. 2006; Speziale et al. 2008; Renaudin et al. 2010; Manzano et al. 2012), suggest that: *a)* the hydrogen bonds play an important role for the structural stability of ettringite, but clarification of this role is obscured by the difficulties in locating the protons and thence of refining the bond distances (*i.e.*, O-H) and angles (*i.e.*, O-H···O), *b)* inter-column H_2O could be disordered, but it is still unclear the nature of the disorder (static or dynamic?) and why the H_2O content is found to vary between 24 and 26 molecules per formula unit (*p.f.u.*) (Manzano et al. 2012). In the framework of a long-term project on the sulphate compounds occurring in cements, we have previously described the mechanisms (at the atomic scale) that stabilize the thaumasite structure at low temperature, giving a clue about the reason of the pronounced sulphate attack of Portland cements observed in cold regions (Gatta et al. 2012). To extend our investigations on the second most important compound, which governs the low-*T* sulphate attack in cements, the aim of the present study is a re-investigation of the crystal structure and crystal chemistry of a natural ettringite at low-*T* by means of single-crystal neutron diffraction, infrared spectroscopy and electron microprobe analysis in wavelength-dispersive mode, to define: *a)* the reliable location of all the proton sites and the real topological configuration of the H_2O and (OH)-groups, for a full description of the atomic relationship *via* the H-bonds; *b)* the anisotropic displacement parameters of the H-sites; *c)* the nature of the disordered distribution of the H_2O molecules into structure, and its potential role on the stability of ettringite.

Experimental methods

The sample description used in this study, along with the characterization protocols by electron microprobe analysis in wavelength-dispersive mode, powder infrared spectroscopy and anisotropic structure refinement, based on single-crystal neutron diffraction data collected at 20 K, are reported in a section of the Supplementary Materials (*deposited*).

----------***[Supplementary Materials - Deposited]*** ----------

Experimental methods:

1) Sample characterization

Ettringite was separate from a specimen from the N'Chwaning mine, Kuruman, Cape Province, Republic of South Africa. The sample (NRM#19950132) is deposited in the mineral collections at the Swedish Museum of Natural History. Large (up to 1.5 cm in length) prismatic, yellow crystals of ettringite and large (up to 1 cm), euhedral, black crystals of braunite-2Q are set on a matrix of fine- to medium-sized (up to 1 mm), pale-red, granular grains of andradite and fine-grained clinochlore.

Electron microprobe analyses were obtained by wavelength dispersive spectroscopy (EPMA–WDS) with a Cameca SX50 instrument at the "Istituto di Geologia Ambientale e Geoingegneria, CNR" of Rome, Italy, using the following analytical conditions: accelerating voltage 15 kV, beam current 15 nA, nominal beam diameter 1 μm. Counting time for one spot analysis was 20 s per peak. Standards (element) are: barite (S and Ba), corundum (Al), wollastonite (Ca and Si), magnetite (Fe), rutile (Ti), rhodonite (Mn), jadeite (Na). The PAP routine was applied (Pouchou and Pichoir 1991) for correction of recorded raw data. Ten spot analyses were performed. The studied grain was found to be homogeneous. Chemical data are given in Table 1 (deposited).

Ettringite is unstable under the electron beam, showing loss of water, which results in significantly higher concentrations for the remaining constituents. Therefore, Table 1 reports also "normalized" constituents to provide a total of 100 wt%, when combined with the H_2O content calculated on the basis of the neutron structure refinement. The empirical formula, based on 51 anions per formula unit, is: $(Ca_{6.07}Na_{0.01})_{\Sigma 6.08}(Al_{1.95}Fe^{3+}_{0.01}Si_{0.01})_{\Sigma 1.97}(SO_4)_{2.99}(OH)_{12}\cdot 27H_2O$.

2) Infrared Spectroscopy

Due to the unstable character of ettringite, no polished single-crystal absorber could be prepared. Attempts to do so resulted in milky crystal slabs, which indicated loss of water. An unpolarized IR spectrum of powdered ettringite in a pressed KBr pellet was recorded in the 600-8000 cm^{-1} at a spectral resolution of 4 cm^{-1} during 32 cycles with a Bruker Vertex 70 microscope spectrometer equipped with a glow-bar source, a KBr beam-splitter, and a mid-band MCT detector. A disc of pure pressed KBr prepared under the same conditions was used as a standard. The recorded spectrum is shown in Figure 2.

3) Neutron diffraction experiment and structure refinement

A first set of single-crystal neutron diffraction data were collected from a large euhedral fragment of ettringite (approx. 12 mm^3) at a temperature of 20 K on the four-circle diffractometer D9 at the Institut Laue-Langevin (ILL), Grenoble. The wavelength used was 0.8403(1) Å obtained from a Cu(220) monochromator and 1500 reflections were measured with a small two-dimensional area detector up to $2\theta_{max}$ = 84.6°, and reduced to 739 unique reflections (Gatta and Fernández-Díaz 2018). The integration, background and Lorentz factor correction of the scans were done with the program

RACER (Wilkinson et al. 1988). To complete the structural information, the same crystal was placed on a close-cycle refrigerator on the monochromatic four-circle diffractometer D19 at ILL. The wavelength used was 1.454(1) Å, provided by a flat Cu(220) monochromator at $2\theta_M = 69.91°$ take-off angle. The sample was cooled to 20 K at 2 K/min cooling rate. The measurement strategy consisted of 22 ω-scans with steps of 0.07° at different χ and φ positions (Fernández-Díaz and Cañadillas-Delgado 2018); reflections up to $2\theta_{max} = 140.4°$ were collected ($\sin\theta/\lambda = 0.597$, max resolution: 0.84 Å). The Multi-Detector Acquisition Data Software (MAD) from ILL was used for data collection. Unit-cell determination [a = 11.171(1) Å, c = 21.364(1) Å] was done by using the PFIND and DIRAX programs, and processing of the raw data was performed using the RETREAT and RAFD19 programs (McIntyre and Stansfield 1988; Duisenberg 1992). Absorption corrections were applied using the D19ABS program (Matthewman et al. 1982). A total number of 14771 Bragg reflections were collected, out of which 1745 reflections were unique for symmetry (R_{int} = 0.0534, Laue class -31m). Initial structural refinements with SHELX-97 (Sheldrick 1997) showed that extinction was pronounced, but could be reasonably well accounted for by the Larson-like correction (Larson 1967). Other details of the data collections are listed in the CIF (deposited).

After preliminary checks about the consistency of the symmetry of the structure models previously reported and the diffraction pattern of this study, the anisotropic structure refinement was performed in the space group $P31c$ using the SHELX-97 software (Sheldrick 1997), starting from the structure model of More and Taylor (1970), without any H sites. The neutron scattering lengths of Ca, Al, S, O and H were used according to Sears (1986). Secondary isotropic extinction effects were corrected according to Larson's formalism (1967), as implemented in the SHELXL-97 package

(Sheldrick 1997). Intense negative residual peaks were found in the difference-Fourier synthesis of the nuclear density when convergence was achieved. Further cycles of refinement were then performed assigning H to these residual peaks (as hydrogen has a negative neutron scattering length). Convergence was slowly achieved and the final least-square cycles were conducted with anisotropic displacement parameters for all the H sites. All the principal mean-square atomic displacement parameters were positively defined. At the end of the last cycle of refinement, no peak larger than –1.2/+2.2 fm/Å^3 was present in the final difference-Fourier map of the nuclear density (maximum and minimum located near the "disordered" inter-column H_2O sites, see next session and Fig. 3) and the variance-covariance matrix showed no significant correlation among the refined parameters. The structure was refined to R_1 = 0.0881 using 381 refined parameters and 1664 unique reflections with $F_o > 4\sigma(F_o)$. Further details pertaining to the structure refinement (statistical parameters, fractional atomic coordinates and displacement parameters) are reported in the CIF. Relevant bond lengths and angles are listed in Table 2 (deposited).

Discussion and Implications

The EPMA–WDS analysis is consistent with the crystal chemistry of ettringite obtained in the previous studies, which is unusual in minerals: it contains about 47 wt% H_2O, 19 wt% SO_3, 27 wt% CaO and 8 wt% Al_2O_3, giving a density of only ~1.83 g/cm^3. Minor content of Mn, Fe, Si and Ti (in total < 0.02 *a.p.f.u.*, potentially replacing Al, Table 1), along with Na and Ba (in total < 0.02 *a.p.f.u.*, potentially replacing Ca, Table 1), are observed. In other words, ettringite from the N'Chwaning mine shows a composition very close to the end-member formula: $Ca_6Al_2(SO_4)_3(OH)_{12}\cdot 27H_2O$.

The neutron structure refinement based on the data collected at 20 K is consistent with the general structure model previously obtained (Moore and Taylor 1968, 1970; Goetz-Neunhoeffer and Neubauer 2006; Hartman and Berliner 2006). The present data show that all twenty crystallographically unique oxygen sites in the ettringite structure are involved in hydrogen bonding:

- OW5-OW12, OW19 and OW20 are H_2O-molecule oxygen atoms. OW5-OW11 belong to the coordination shell of two Ca sites (*i.e.*, Ca1: OW6, OW8, OW10, OW12; Ca2: OW5, OW7, OW9, OW11; Fig. 1, see also the CIF). All the H_2O molecules are H bonded, with the following energetically favurable configurations: OW5-H3···O18 (*i.e.*, O18 belonging to a SO_4-group), OW5-H7···O15 (*i.e.*, O15 belonging to a SO_4-group), OW6-H1···O15, OW6-H6···O18, OW7-H12···O16 (*i.e.*, O16 belonging to a SO_4-group), OW7-H17···OW19 (or OW20) (*i.e.*, H_2O···H_2O interaction), OW8-H11···O16, OW8-H13···OW19 (or OW20), OW9-H15···O16, OW9-H16···O15, OW10-H2···O18, OW10-H20···O14 (*i.e.*, O14 belonging to a SO_4-group), OW11-H9···OW9 (*i.e.*, OW9 belonging to a Ca-polyhedron, H_2O···H_2O interaction), OW11-H19···O17 (*i.e.*, O17 belonging to a SO_4-group), OW12-H10···O13 (*i.e.*, O13 belonging to a SO_4-group), OW12-H18···OW10 (*i.e.*, OW10 belonging to a Ca-polyhedron, H_2O···H_2O interaction), OW19-H21···OW19 (or OW20), OW19-H23···OW12 (*i.e.*, OW12 belonging to a Ca-polyhedron, H_2O···H_2O interaction), OW20-H22···OW11 (*i.e.*, OW11 belonging to a Ca-polyhedron, H_2O···H_2O interaction), OW20-H24···OW12 (Table 2). All the H bonds show O···O distances ranging between 2.66 and 2.98 Å (Table 2).
- OH1-OH4 are oxygen atoms of hydroxyl groups, and belong to the coordination shell of the two unique Al sites (Fig. 1, see also the CIF). The

oxygen atoms of the hydroxyl groups act as donors, forming H-bonds with the H_2O oxygen sites (all belonging to the Ca-coordination shells) as acceptors (*i.e.*, OH1-H8···OW5, OH2-H5···OW6, OH3-H14···OW7 and OH4-H4···OW8, Table 2). All the H-bonds show O···O distances ranging between 3.1 and 3.2 Å (Table 2).

All the building-block units of the ettringite structure [*i.e.*, SO_4 groups, $Al(OH)_6$ octahedra and $Ca(OH)_4(H_2O)_4$ polyhedra] are connected *via* H bonds.

The geometry of the H_2O molecule is now well defined: the O-H distances corrected for "riding motion" (Busing and Levy 1964) range between 0.96 and 1.07 Å (Table 2). The H-OW-H angles range between 101.7-109.7° (Table 2), and are all still in the range of the observed H-O-H angles in solid-state materials (Chiari and Ferraris 1982; Steiner 1998 and references therein; Gatta et al. 2008). For the hydroxyl groups, the O-H distances corrected for "riding motion" range between 0.94-1.02 Å (Table 2). All the hydrogen bonds show O-H···O angles ≥ 160° (Table 2), a configuration which is energetically less costly (*i.e.*, approaching linearity, Steiner 1998), if compared to that of other minerals (*e.g.*, phyllosilicates, with O-H···O angles ranging between 120°-140°; Gatta et al. 2011, 2013). The oxygen and hydrogen atoms of the H_2O molecules and (OH) groups have slightly larger anisotropic displacement parameters if compared to the other sites populated by Ca, Al or Si; the maximum ratio of the *max* and *min* root-mean-square components of the displacement ellipsoid is observed for the protons of the hydroxyl groups (*i.e.*, OH1-OH4). However, the magnitude of the displacement ellipsoids of the non-H_2O atoms is somehow mitigated by the low *T*.

The different Fourier-map of the nuclear density shows a disordered distribution of the inter-column "free" H_2O molecules of the ettringite structure, which was modelled (in the structure refinement) with two independent and mutually exclusive

258 configurations: H21-OW19-H23 and H22-OW20-H24 (Fig. 3, see also the CIF). In the
259 structure refinement, the best fit was obtained with *s.o.f.* of 0.48(1) and 0.52(1) for each
260 configuration (then fixed to 0.5 for each one in the last cycles of refinement), leading to
261 a total number of 27 H_2O molecules *p.f.u.*. OW19 and OW20 act as "inter-column
262 bridges", between the Ca-polyhedra (Table 2). As the disorder is still preserved down to
263 20 K, we are inclined to consider that as a "static disorder". We cannot exclude that the
264 H-bonding network of the H_2O molecules promotes the disorder, at least partially: for
265 each of the two configurations (*i.e.*, OW19 and OW20), one of the two protons has an
266 almost ideal H-bonding geometry, the other one not (*i.e.*, with OW-H···O ranging
267 between 162-170° *vs.* 144-147°, Table 2). The refined isotropic displacement
268 parameters of the inter-column H_2O sites are likely affected by the positional disorder
269 (presumably overestimated; see the CIF). With the disordered configuration here
270 observed, there is no domain of the structure without the presence of inter-column H_2O
271 molecules, and thus we cannot expect a relevant role of the disorder on the stability of
272 the structure under non-ambient conditions. Furthermore, ettringite with less than 27
273 H_2O molecules *p.f.u.*, if it exists, would behave differently at non-ambient conditions.
274 The structure refinement shows that, in the ettringite structure, the SO_4 tetrahedra
275 are slightly distorted, with $\Delta(S\text{-}O)_{max} \sim 0.015$ Å (*i.e.*, the difference between the longest
276 and the shortest bond distances), and the $\Delta(O\text{-}S\text{-}O)_{max} \sim 1.5°$ (*i.e.*, the difference
277 between the highest and the lowest intra-tetrahedral angle). The $Al(OH)_6$ octahedra are
278 more distorted, with $\Delta(Al1\text{-}O)_{max}$ and $\Delta(Al2\text{-}O)_{max} \sim 0.045$ Å. The $Ca(OH)_4(H_2O)_4$
279 polyhedra are highly distorted, with $\Delta(Ca1\text{-}O)_{max} \sim 0.217$ Å and $\Delta(Ca2\text{-}O)_{max} \sim 0.283$ Å
280 (Table 2).
281 The recorded infrared spectrum of ettringite (Fig. 2) shows an intense and broad
282 absorption in the range 3150-3750 cm^{-1} with a maximum at 3427 cm^{-1}. This feature is

283 overprinted by a relatively narrow band at 3638 cm^{-1}. In accordance with the detailed
284 experimental and theoretical analysis of the ettringite vibrational spectra by Scholtzova
285 et al. (2015), the broad absorption feature is assigned to O-H stretching in H_2O, while
286 the narrow band at higher wavenumbers is ascribed to O-H stretching modes in (OH)-
287 groups from the $Al(OH)_6$-octahedra. Absorption at 1640 and 1680 cm^{-1} are caused by
288 bending modes in H_2O. In addition, several absorption bands are observed at lower
289 wavenumbers (*i.e.*, 620, 755, 855, 990 and 1114 cm^{-1}). The recorded spectrum is similar
290 to those previously reported (*e.g.*, Frost et al. 2013; Scholtzova et al. 2015). The
291 assignment of the observed bands, based on the work by Scholtzova et al. (2015), is
292 summarized in Table 3. The splitting of the H-O-H bending mode was explained by
293 Scholtzova et al. (2015) by the presence of the "non-equivalent" H_2O molecules in the
294 crystal structure, related to different hydrogen bond strength and different structural
295 environment. Typical absorption bands in the range 1200-1250 cm^{-1} caused by $B(OH)_4$-
296 groups in ettringite group minerals (Chukanov and Chervonnyi 2016) are not observed
297 in the spectrum of the present sample.

298 Diffraction and spectroscopic findings of this study suggest that the structural
299 stability of ettringite is mainly governed by the hydrogen-bonding geometry, as all of
300 the major building units (*i.e.*, SO_4, $Al(OH)_6$, Ca-polyhedra) are held together by
301 hydrogen bonds. Similar findings were reported for thaumasite (Gatta et al. 2012). This
302 can explain the modest stability of ettringite at high temperature (with structure
303 collapsing at $T < 150$ °C; Zhou and Glasser 2001) or at high pressure (evidence of
304 amorphization were observed at $P \sim 3$ GPa; Clark et al. 2008), likely reflecting the
305 incapacity of the H-bonding scheme to be preserved even at modest high-
306 temperature/high-pressure conditions. In contrast, low T stabilizes the ettringite
307 structure, as corroborated by the H-bonding configuration, similarly to what already

observed for thaumasite (Gatta et al. 2012). We can then extend even to ettringite the same considerations reported by Gatta et al. (2012) on thaumasite: pronounced sulphate attack of Portland cements, observed in cold regions, takes place likely in response to favorable nucleation and growth of ettringite and thaumasite under such conditions. However, whereas the sulphate attack of cement promoted by percolation of sulphate-rich fluids can be potentially mitigated, by isolating the cement structures, it is difficult to prevent the delayed formation of ettringite and thaumasite promoted by the chemical components that already occur in cement paste.

We expect that the revised structural model, here obtained, will be employed for a more efficient identification and quantification of ettringite in polyphasic mixtures such as Portland cements. In addition, as the ettringite crystal morphology was observed to affect the expansion of cement structures (Tosun and Baradan 2010), the structure model here derived would deliver a valuable contribution to investigate any potential correlation between the ettringite's habit and its crystal structure, for example *via* periodic-bond-chain development (*e.g.*, Hartman and Chan 1993).

Acknowledgements

The authors thank the Institut Laue-Langevin, Grenoble (France), for the allocation of neutron beam time. The Editor, Ian Swainson, and four anonymous reviewers are thanked. GDG acknowledge the support of the Italian Ministry of Education (MIUR) through the project 'Dipartimenti di Eccellenza 2018-2022'.

References

Asamoto, S., Murano, K., Kurashige, I., and Nanayakkara, A. (2017) Effect of carbonate ions on delayed ettringite formation. Construction and Building Materials, 147, 221–226.

Barnett, S.J., Adam, C.D., and Jackson, A.R.W. (2000) Solid solutions between ettringite, $Ca_6Al_2(SO_4)_3(OH)_{12}\cdot 26H_2O$, and thaumasite $Ca_3SiSO_4CO_3(OH)_6\cdot 12H_2O$. Journal of Material Science, 35, 4109–4114.

Bensted, J. (1999) Thaumasite — background and nature in deterioration of cements, mortars and concretes. Cement and Concrete Composites, 21, 117–121.

Busing, W.R. and Levy, H.A. (1964) The effect of thermal motion on the estimation of bond lengths from diffraction measurements. Acta Crystallographica, 17, 142–146.

Chiari, G. and Ferraris, G. (1982) The water molecules in crystalline hydrates studied by neutron diffraction. Acta Crystallographica, B38, 2331–2341.

Chukanov, N.V. and Chervonnyi, A.D. (2016) Infrared Spectroscopy of Minerals and Related Compounds. Springer International Publishing Switzerland.

Clark, S.M., Colas, B., Kunz, M., Speziale, S., and Monteiro, P.J.M. (2008) Effect of pressure on the crystal structure of ettringite. Cement and Concrete Research, 38, 19–26.

Crammond, N.J. (1985) Thaumasite in failed cement mortars and renders from exposed brickwork. Cement Concrete Research, 15, 1039–1050.

Deb, S.K., Manghnani, M.H., Ross, K., Livingston, R.A., and Monteiro, P.J.M. (2003) Raman scattering and X-ray diffraction study of the thermal decomposition of an ettringite-group crystal. Physics and Chemistry of Minerals, 30, 31-38.

Duisenberg, A.J.M. (1992) Indexing in single-crystal diffractometry with an obstinate list of reflections. Journal of Applied Crystallography, 25, 92–96.

Fernández-Díaz, M.T. and Cañadillas-Delgado, L. (2018) Structure of ettringite; Experimental Report - Institut Laue-Langevin (ILL): Grenoble, 2018; DOI: 10.5291/ILL-DATA.TEST-2828.

Frost, R.L., López, A., Xi, Y., Scholz, R., Magela da Costa, G., Fernandes Lima, R.M., and Granja, A. (2013) The spectroscopic characterization of the sulphate mineral ettringite from Kuruman manganese deposits, South Africa. Vibrational Spectroscopy, 68, 266–271.

Gatta, G.D. and Fernández-Díaz, M.T. (2018) New insight into the crystal structure of ettringite: $Ca_6[Al(OH)_6]_2(SO4)_3 \cdot 26H_2O$; Experimental Report - Institut Laue-Langevin (ILL): Grenoble, 2018; DOI: 10.5291/ILL-DATA.5-11-419.

Gatta, G.D., Rotiroti, N., McIntyre, G.J., Guastoni, A., and Nestola, F. (2008) New insights into the crystal chemistry of epididymite and eudidymite from Malosa, Malawi: a single-crystal neutron diffraction study. American Mineralogist, 93, 1158–1165.

Gatta, G.D., McIntyre, G.J., Sassi, R., Rotiroti, N., and Pavese, A. (2011) Hydrogen-bond and cation partitioning in $2M_1$-muscovite: A single-crystal neutron-diffraction study at 295 and 20 K. American Mineralogist, 96, 34–41.

Gatta, G.D., McIntyre, G.J., Swanson, G.J., and Jacobsen, S.D. (2012) Minerals in cement chemistry: a single-crystal neutron diffraction and Raman spectroscopic study of thaumasite, $Ca_3Si(OH)_6(CO_3)(SO_4) \cdot 12H_2O$. Am. Mineral., 97, 1060–1069.

Gatta, G.D., Merlini, M., Valdrè, G., Liermann, H-P., Nénert, G., Rothkirch, A., Kahlenberg, V., and Pavese, A. (2013) On the crystal structure and compressional

382 behaviour of talc: a mineral of interest in petrology and material science. Physics
383 and Chemistry of Minerals, 40, 145–156.
384 Goetz-Neunhoeffer, F. and Neubauer, J. (2006) Refined ettringite
385 ($Ca_6Al_2(SO_4)_3(OH)_{12}\cdot 26H_2O$) structure for quantitative X-ray diffraction analysis.
386 Powder Diffraction, 21, 4–11.
387 Hartman, M.R., and Berliner, R. (2006) Investigation of the structure of ettringite by
388 time-of-flight neutron powder diffraction techniques. Cement and Concrete
389 Research, 36, 364–370.
390 Hartman, M.R., Brady, S.K., Berliner, R., and Conradi, M.S. (2006) The evolution of
391 structural changes in ettringite during thermal decomposition. Journal of Solid
392 State Chemistry, 179, 1259–1272.
393 Hartman, P., and Chan, H-K. (1993) Application of the Periodic Bond Chain (PBC)
394 Theory and Attachment Energy Consideration to Derive the Crystal Morphology
395 of Hexamethylmelamine. Pharmaceutical Research, 10, 1052–1058.
396 Hartshorn, S.A., Sharp, J.H., and Swamy, R.N. (1999) Thaumasite formation in
397 Portland limestone cement pastes. Cement Concrete Research, 29, 1331–1340.
398 Hobbs, D.W. and Taylor, M.G. (2000) Nature of the thaumasite sulphate attack
399 mechanism in field concrete. Cement and Concrete Research, 30, 529–533.
400 Larson, A.C. (1967) Inclusion of secondary extinction in least-squares calculations.
401 Acta Crystallographica, 23, 664 – 665.
402 Manzano, H., Ayuela, A., Telesca, A., Monteiro, P.J.M. and Dolado, J.S. (2012)
403 Ettringite strengthening at high pressures induced by the densification of the
404 hydrogen bond network. Journal of Physical Chemistry, C116, 16138-16143.

405 Matthewman, J.C., Thompson, P., and Brown, P.J. (1982) The Cambridge
406 Crystallography Subroutine Library. Journal of Applied Crystallography, 15, 167–
407 173.
408 McIntyre, G.J., and Stansfield, R.F.D. (1988) A general Lorentz correction for single-
409 crystal diffractometers. Acta Crystallographica, A44, 257-262.
410 Moore, A. and Taylor, H.F.W. (1968) Crystal structure of ettringite. Nature, 218, 1048–
411 1049.
412 Moore, A. and Taylor, H.F.W. (1970) Crystal structure of ettringite. Acta
413 Crystallographica, B26, 386–393.
414 Pouchou, J.L. and Pichoir, F. (1991) Quantitative Analysis of Homogeneous or
415 Stratified Microvolumes Applying the Model “PAP”. In: Heinrich, K.F.J. and
416 Newbury, D.E., Eds., Electron Probe Quantification, Plenum Press, New York,
417 31–75.
418 Renaudin, G., Sengi, R., Mentel, D., Nedelec, J.M., Leroux, F., and Taviot-Gueho, C.
419 (2007) A Raman study of the sulfated cement hydrates: ettringite and
420 monosulfoaluminate. Journal of Advanced Concrete Technology, 5, 299–312.
421 Renaudin, G., Filinchuk, Y., Neubauer J., Goetz-Neunhoeffer, F. (2010) A comparative
422 structural study of wet and dried ettringite. Cement and Concrete Research, 40,
423 370–375.
424 Santhanam, M., Cohen, M.D., and Olek, J. (2001) Sulfate attack research – wither now?
425 Cement and Concrete Research, 31, 845–851.
426 Scholtzová, E., Kucková, L., Kožíšek J., and Tunega, D. (2015) Structural and
427 spectroscopic characterization of ettringite mineral - combined DFT and
428 experimental study. Journal of Molecular Structure, 1100, 215–224.

Sears, V.F. (1986) Neutron Scattering Lengths and Cross-Sections. In K. Sköld and D.L. Price, Eds., Neutron Scattering, Methods of Experimental Physics, Vol. 23A, p. 521-550. Academic Press, New York.

Sheldrick, G.M. (1997) SHELX-97. Programs for crystal structure determination and refinement. University of Göttingen, Germany.

Skoblinskaya, N.N. and Krastlnikov, K.G. (1975) Changes in crystal structure of ettringite on dehydration. Part 1. Cements and Concretes Research, 5, 381–394.

Skoblinskaya, N.N., Krastlnikov, K.G., Nikitina, L.V., and Varlamov, V.P. (1975) Changes in crystal structure of ettringite on dehydration. Part 2. Cement and Concrete Research, 5, 419–432.

Speziale, S., Jiang, F., Mao, Z., Monteiro, P.J.M., Wenk, H-R., Duffy, T.S., and Schilling, F.R. (2008) Single-crystal elastic constants of natural ettringite. Cement and Concrete Research, 38, 885–889.

Steiner, T. (1998) Opening and narrowing of the water H-O-H angle by hydrogen-bonding effects: Re-inspection of neutron diffraction data. Acta Crystallographica, B54, 464-470.

Taylor, H.F.W. (1997) Cement Chemistry, second ed., Thomas Telford, London, 1997.

Tosun, K., and Baradan, B. (2010) Effect of ettringite morphology on DEF-related expansion. Cement and Concrete Composites, 32, 271–280.

Wilkinson, C., Khamis, H.W., Stansfield, R.F.D., and McIntyre, G.J. (1988) Integration of single-crystal reflections using area multidetectors. Journal of Applied Crystallography, 21, 471–478.

Zhang, F.C., Ma, B.G, Yin, G., Wu, Y.Y., and Zhu, Y.C. (2009) Preparation and performance of sulfate resistance cement-based material. Key Engineering Materials, 400, 195–201.

454 Zhou, Q., and Glasser, F.P. (2001) Thermal Stability and Decomposition Mechanisms
455 of Ettringite at < 120°C. Cement and Concrete Research, 31, 1333–1339.
456

Table 1 [deposited]. Chemical data for ettringite NRM#19950132, based on EPMA-WDS data and neutron structure refinement.

	Measured	Normalized
Na_2O (wt%)	0.04(2)	0.03
CaO	38.7(5)	26.7
BaO	0.01(1)	0.01
Al_2O_3	11.3(2)	7.81
Mn_2O_3	0.02(2)	0.01
Fe_2O_3	0.06(4)	0.04
SiO_2	0.05(5)	0.04
TiO_2	0.01(1)	0.01
SO_3	27.2(6)	18.8
H_2O*		46.55
Total	77.47	100
Number of cations on the basis of 51 anions		
Na (*a.p.f.u.*)		0.010
Ca		6.070
Ba		0.001
Al		1.954
Mn^{3+}		0.002
Fe^{3+}		0.007
Si		0.008
Ti^{4+}		0.001
S^{6+}		2.987
H^+		66.000

Note: Errors for oxides are standard deviations (in brackets) of several spot analyses; *a.p.f.u.* = atoms per formula unit.
*H_2O content according to the neutron structure refinement: 27 H_2O molecules *p.f.u.*

Table 2 [deposited]. Relevant bond distances (Å) and angles (°) for ettringite based on the neutron structure refinement (data collected at 20 K).

Al1-OH1 (x3)	1.885(9)	OH1-Al1-OH1	87.2(6)	OH3-Al2-OH3	87.3(6)		
Al1-OH2 (x3)	1.928(10)	OH1-Al1-OH2	178.7(7)	OH3- Al2-OH4	95.6(2)		
Al2-OH3 (x3)	1.877(9)	OH1-Al1-OH2	94.1(2)	OH3- Al2-OH4	92.2(2)		
Al2-OH4 (x3)	1.923(10)	OH1-Al1-OH2	93.3(2)	OH3-Al2-OH4	177.0(4)		
Ca1-OH3	2.416(5)	OH2-Al1-OH2	85.5(6)	OH4-Al2-OH4	85.0(6)		
Ca1-OH1	2.418(6)						
Ca1-OW6	2.443(7)						
Ca1-OW8	2.443(7)	O13-S1-O15	110.2(3)	O17-S3-O18	108.9(3)		
Ca1-OH1	2.459(5)	O15-S1-O15	108.8(3)	O18-S3-O18	110.0(4)		
Ca1-OH3	2.462(6)						
Ca1-OW10	2.603(5)	O14-S2-O16	109.2(4)				
Ca1-OW12	2.633(5)	O16-S2-O16	109.7(4)				
Ca2-OH4	2.379(5)						
Ca2-OH2	2.407(5)						
Ca2-OH2	2.408(5)						
Ca2-OH4	2.409(5)						
Ca2-OW5	2.432(6)						
Ca2-OW7	2.440(6)						
Ca2-OW9	2.614(4)						
Ca2-OW11	2.662(4)						
S1-O15 (x3)	1.481(4)						
S1-O13	1.491(7)						
S2-O14	1.481(8)						
S2-O16 (x3)	1.486(4)						
S3-O18 (x3)	1.474(4)						
S3-O17	1.490(8)						
OH1-H8	0.973(9)	OW5-H3	0.991(6)	OW5-H7	0.988(8)		
OH1-H8*	1.000(12)	OW5-H3*	1.007(9)	OW5-H7*	1.001(11)		
H8···OW5	2.170(10)	H3···O18	1.780(6)	H7···O15	1.841(9)		
OH1···OW5	3.098(5)	OW5···O18	2.749(4)	OW5···O15	2.822(6)		
OH1-H8···OW5	159.2(7)	OW5-H3···O18	164.8(6)	OW5-H7···O15	171.4(6)		
OH2-H5	0.903(9)	OW6-H1	0.926(6)	OW6-H6	0.937(9)		
OH2-H5*	0.920(11)	OW6-H1*	0.943(9)	OW6-H6*	0.962(12)		
H5···OW6	2.223(9)	H1···O15	1.845(7)	H6···O18	1.890(10)		
OH2···OW6	3.105 (6)	OW6···O15	2.748(4)	OW6···O18	2.805(6)		
OH2-H5···OW6	165.3(7)	OW6-H1···O15	164.3(7)	OW6-H6···O18	164.5(8)		
OH3-H14	0.952(9)	OW7-H12	0.959(9)	OW7-H17	0.954(7)		
OH3-H14*	0.980(12)	OW7-H12*	0.981(12)	OW7-H17*	0.982(10)		
H14···OW7	2.225(10)	H12···O16	1.835(10)	H17···O20	1.734(11)	H17···O19	1.856(11)
OH3···OW7	3.136(6)	OW7···O16	2.779(6)	OW7···O20	2.662(8)	OW7···O19	2.734(7)
OH3-H14···OW7	159.7(7)	OW7-H12···O16	167.5(8)	OW7-H17···O20	163.2(9)	OW7-H17···O19	151.7(8)
OH4-H4	0.936(9)	OW8-H11	0.927(10)	OW8-H13	0.940(9)		
OH4-H4*	0.963(12)	OW8-H11*	0.959(14)	OW8-H13*	0.987(12)		
H4···OW7	2.269(9)	H11···O16	1.824(11)	H13···O19	1.928(12)	H13···O20	2.203(13)
OH4···OW7	3.179(6)	OW8···O16	2.738(6)	OW8···O19	2.822(7)	OW8···O20	3.047(9)
OH4-H4···OW7	163.8(6)	OW8-H11···O16	167.9(9)	OW8-H13···O19	158.2(9)	OW8-H13···O20	149.0(9)
		OW9-H15	0.904(9)	OW9-H16	0.934(8)		
		OW9-H15*	0.930(12)	OW9-H16*	0.951(11)		
		H15···O16	1.804(9)	H16···O15	1.829(8)		
		OW9···O16	2.702(5)	OW9···O15	2.761(5)		
		OW9-H15···O16	172.0(8)	OW9-H16···O15	175.9(7)		
		OW10-H2	0.996(7)	OW10-H20	1.013(9)		
		OW10-H2*	1.016(9)	OW10-H20*	1.039(12)		
		H2···O18	1.816(7)	H20···O14	1.931(8)		
		OW10···O18	2.803(5)	OW10···O14	2.906(5)		
		OW10-H2···O18	170.6(6)	OW10-H20···O14	160.6(7)		
		OW11-H9	0.957(10)	OW11-H19	0.959(8)		
		OW11-H9*	0.967(13)	OW11-H19*	0.975(12)		
		H9···OW9	2.029(11)	H19···O17	1.879(8)		
		OW11···OW9	2.981(7)	OW11···O17	2.821(5)		

OW11-H9···OW9	172.9(8)	OW11-H19···O17	166.8(6)		
OW12-H10	0.927(9)	OW12-H18	0.926(14)		
OW12-H10*	0.957(12)	OW12-H18*	0.968(18)		
H10···O13	1.937(10)	H18···OW10	2.068(15)		
OW12···O13	2.835(5)	OW12···OW10	2.983(6)		
OW12-H10···O13	162.6(8)	OW12-H18···OW10	169.1(11)		
OW19-H21	0.982(9)	OW20-H22	0.986(9)	OW19···OW20	0.86(1)
OW19-H23	0.988(8)	OW20-H24	0.981(9)		
H21-OW19-H23	104.4(11)	H22-OW20-H24	103.5(12)		
H21···OW19	1.485(15)	H22···OW11	2.042(11)		
OW19···OW19	2.355(11)	OW20···OW11	2.910(10)		
OW19-H21···OW19	144.5(16)	OW20-H22···OW11	145.7(9)		
H21···OW20	1.747(12)	H24···OW12	1.920(10)		
OW19···OW20	2.630(12)	OW20···OW12	2.869(9)		
OW19-H21···OW20	147.6(16)	OW20-H24···OW12	161.7(9)		
H23···OW12	1.859(9)				
OW19···OW12	2.837(9)				
OW19-H23···OW12	169.9(10)				

* Bond distance corrected for “riding motion” following Busing and Levy (1964)

Table 3 [deposited]. Assignments of FTIR-bands in ettringite.

Vibrational mode		*Wavenumber (cm^{-1})*
ν_{as}	$(O\text{-}H)_{Al}$ and $\nu_S(O\text{-}H)_{Al}$	3638
ν_S	$(O\text{-}H)_w$	3427
δ	H-O-H	1680
δ	H-O-H	1640
ν_{as}	S-O	1114
ν_S	S-O and ν_{as} Al-O	990
δ	Al-O-H	855
δ	Al-(O-H)	755
δ	O-S-O	620

Figure 1. (*Top*) The crystal structure of ettringite viewed down [001] based on the neutron structure refinement at 20 K of this study. Displacement-ellipsoid probability factor: 50%. (*Down*) Configuration of the $[Ca_3Al(OH)_6(H_2O)_{12}]$ building-block units forming columns parallel to [001] (*left side*), and of the alternating H_2O and SO_4 tetrahedra running along [001] (*right side*).

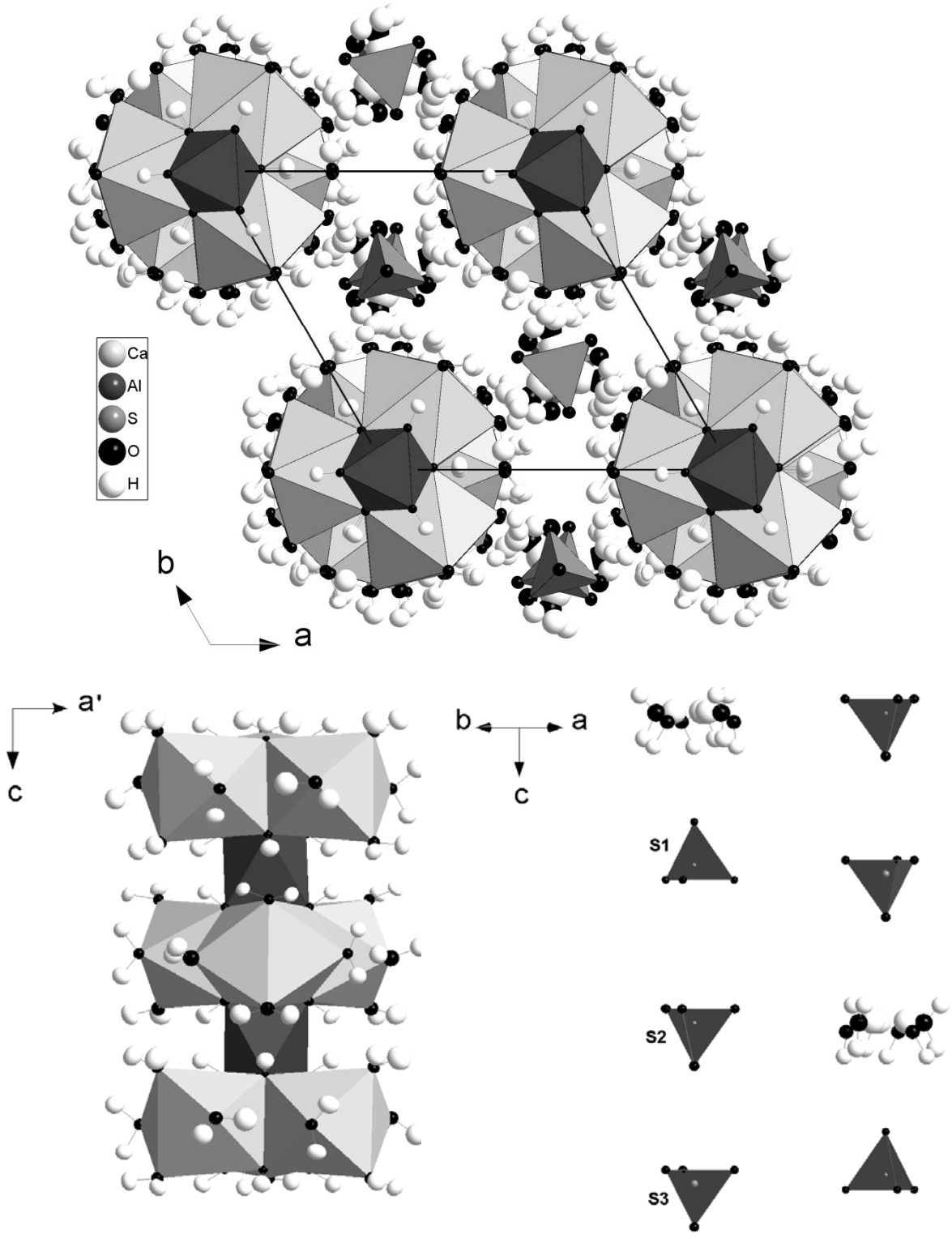

607 Figure 2. Infrared spectrum of ettringite.

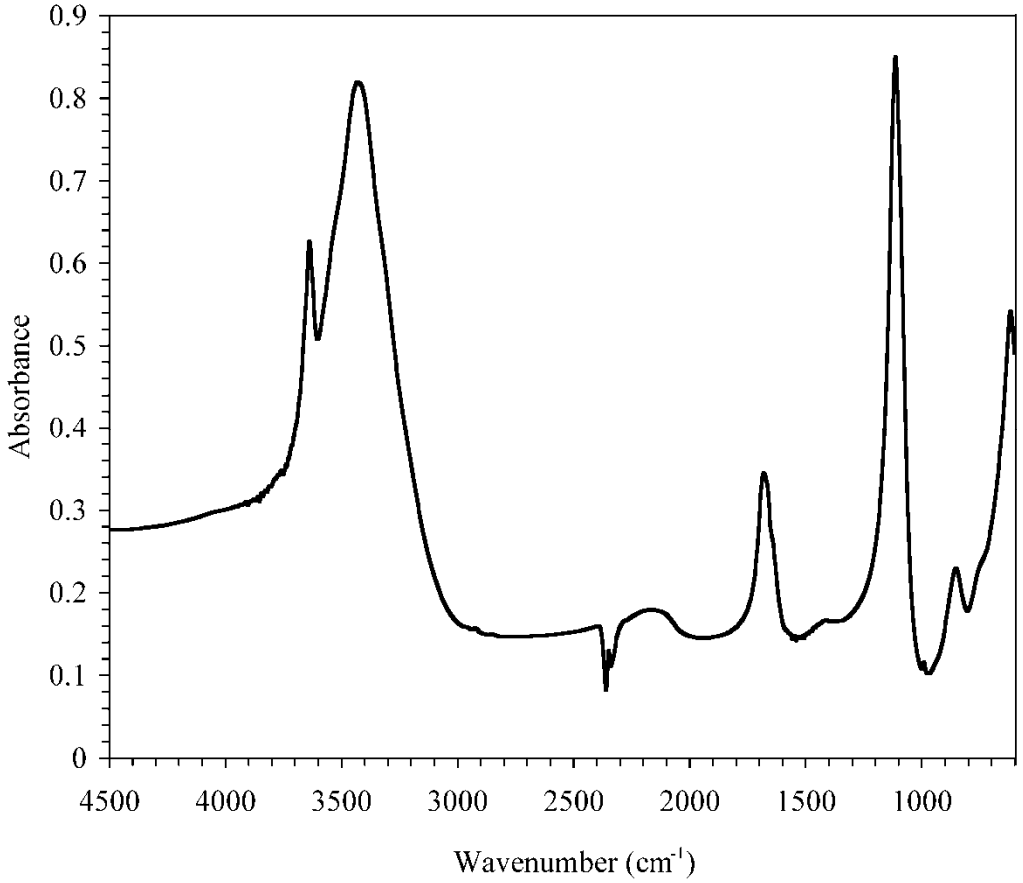

608
609
610
611
612
613
614
615
616
617
618
619
620
621
622
623
624
625
626
627
628
629
630

Figure 3. (*Top*) Difference Fourier maps of ettringite at $z \sim 0.235$ calculated with coefficients *F*o-*F*c and phased by *F*c. The *F*c were calculated from a structural model without the inter-column H_2O sites (H21-OW19-H23, H22-OW20-H24; CIF and Table 2). Maxima, ascribable to the missing O sites, and minima, ascribable to the missing H sites (as H has negative neutron scattering length), about the 3-fold axis, are visible. Color bar unit: fm/Å^3. (*Down*) Schematic configuration and location of the inter-column H_2O sites.